CrystEngComm

RSC Publishing

PAPER

View Article Online
View Journal | View Issue

High-speed ultraviolet-visible-near infrared photodiodes based on p-ZnS nanoribbon–n-silicon heterojunction

Cite this: *CrystEngComm*, 2013, **15**, 1635

Yong-Qiang Yu,[ab] Lin-Bao Luo,*[b] Zhi-Feng Zhu,[ab] Biao Nie,[b] Yu-Gang Zhang,[ab] Long-Hui Zeng,[b] Yan Zhang,[ab] Chun-Yan Wu,[b] Li Wang[b] and Yang Jiang*[a]

Received 21st October 2012,
Accepted 24th November 2012

DOI: 10.1039/c2ce26730f

www.rsc.org/crystengcomm

Ag-doped p-type ZnS nanoribbons (NRs) with a high hole concentration of 5.1×10^{18} cm^{-3} and high carrier mobility of 154.0 cm^2 V^{-2} s^{-1} were synthesized by using silver sulfide (Ag_2S) as the Ag source. Excellent ohmic contact to p-ZnS NR with specific contact resistivity as low as 5.6×10^{-7} Ω cm^2 was achieved by using bilayer Cu (4 nm)–Au electrode, which according to the depth profiling X-ray photoelectron spectroscopy (XPS) and Auger electron spectroscopy (AES) analysis can help to form a thin Cu_2S interfacial layer between the electrode. Based on the high quality ZnS NRs and achievement on ohmic contact, p–n photodiodes have been constructed from the p-ZnS nanoribbon (NR)–n-Si heterojunction with a response speed as high as ~48 μs (rise time). Furthermore, the device also exhibits stable optoelectrical properties with high sensitivity to UV-visible-NIR light and an enhancement of responsivities of 1.1×10^3 AW^{-1} for 254 nm under a reverse bias of 0.5 V. These generality of the above results shows that the p-ZnS NR–n-Si heterojunction will have potential applications in future high-performance photodetectors.

Introduction

In the last decade, one-dimensional (1D) semiconductor nanostructures, with large surface-to-volume ratio, small size and quantum confinement size effect have shown great potential as building blocks for optoelectronics, such as lasers,[1] light-emitting diodes (LEDs),[2] solar cells,[3,4] photodetectors (PDs),[5,6] and so on. Thanks to the rapid advancement in the "bottom-up" control growth and development in fabrication methodologies, 1D semiconductor nanostructures have opened huge opportunities to develop various PDs with exceptionally higher sensitivity and quicker response time.[7] In recent studies, high photoconductive gain of the PDs based on 1D nanostructures have been observed on various semiconductors, such as ZnO nanowires (NWs) (~10^8),[8] ZnS nanoribbons (NRs) (~10^7)[9] and InP NWs (~3×10^3).[10] These nano-PDs with high photoconductive gains are believed to be associated with the longer photo-carrier lifetime which originates from the carriers trapping in both bulk defects and surface states.[8] The slower recombination of the photo-carriers makes the device take a much longer time to reach to dark current level, and consequently, a relatively slow photoresponse speed is attained. In practical applications, the PDs must be not only responsive to photo-excitation but also quick to relax to the dark state when the light source is turned off. To this end, photodetector composed of 1D p–n heterojunction nanostructures with high speed, high sensitivity and low operational voltages have been developed. For instance, based on nanoscale avalanche photodiodes (APDs) composed of crossed p-Si–n-CdS nanowire (NW) or InAs–InAsP axial heterojunctions, photodetectors with excellent devices performance have been successfully studied.[11,12] Nonetheless, these devices' fabrication is characterized by accurately controlled synthesis via either sophisticated or expensive instruments which greatly hinders its wide application. As an alternative, the nanostructures–thin film p–n heterojunction with a nanometer junction holds great promise. To date, many efforts have been dedicated to heterojunction PDs composed of 1D wide band gap semiconductors nanostructures on doped Si substrates. By combining wide band gap semiconductors, such as ZnO,[13,14] SnO_2[15] and ZnTe[16] with silicon film, the whole range of light from UV to near-IR (NIR) can be effectively absorbed by this kind of photodiode, which is highly beneficial to wide wavelength application of PDs.

Recently, 1D ZnS nanostructures, as an important II–VI compound semiconductor with a wide band-gap of 3.7 eV at room temperature, have attracted much attention for their wide applications in nano-electronic and nano-optoelectronic devices, such as field emitters,[17] gas sensors,[18] and UV photodetectors (PDs).[19,20] Among these applications, growth

[a]*School of Materials Science and Engineering, Hefei University of Technology, Hefei, Anhui 230009, P. R. China. E-mail: apjiang@hfut.edu.cn*
[b]*School of Electronic Science and Applied Physics, Hefei University of Technology, Hefei, Anhui 230009, P. R. China. E-mail: luolb@hfut.edu.cn*

of high quality p-type ZnS is an important issue for utilization in optoelectronic devices due to the strong self-compensation effect by native vacancies.[21] Meanwhile, reliable ohmic contacts to p-ZnS nanostructures with low contact resistance are an essential issue to improve device performance. The fabrication of effective p-type ZnS nanostructures for heterojunction PDs with good device performance is yet to be demonstrated. In this work, we present the synthesis of p-type ZnS NRs with high carrier mobility by using silver sulfide (Ag_2S) as the Ag source. To achieve ohmic contact to the p-type ZnS NR, a new metallization technique by using bilayer Cu–Au electrode was developed. In addition, the as-fabricated photodiodes exhibited excellent device performance with wide wavelength response from UV to NIR, fast response speed of 48 μs and high responsivity.

Experimental section

Materials synthesis and characterization

In this study, the p-type ZnS NRs were synthesized by using Ag_2S as the dopant *via* a chemical vapor deposition (CVD) method. Briefly, Ag_2S powder was placed at the upstream position at 10 cm distance from the ZnS source (0.3 g, 99.99%, Aldrich) and the molar ratio of Ag_2S : ZnS was 1 : 6. Si substrates coated with a layer of 5 nm gold catalyst were placed downstream ~10 cm away from the ZnS source. The evaporation system was evacuated to a base pressure of 4×10^{-5} Torr, and backfilled with a constant H_2 (5% in Ar) gas flow of 40 sccm to a pressure of 100 Torr. Afterwards, the ZnS source was heated up to 1060 °C in one hour and kept at that temperature for 30 min. The as-synthesized ZnS:Ag NRs were characterized by field-emission scanning electron microscope (FESEM, Philips XL 30 FEG) equipped with X-ray energy dispersive spectrometer (EDS) and cathodoluminescence (CL) system, X-ray diffraction (XRD, Rigaku D/Max-rB), high-resolution transmission electron microscope (HRTEM, JEOL JEM-2010), X-ray photoelectron spectroscopy (XPS) and X-ray-induced Auger electron spectroscopy (XAES) (Thermo ESCALAB 250Xi) equipped with a Al Kα (1486.6 eV) and Ar^+ ion beam.

Device construction and characterization

In order to assess the electrical transport properties of the ZnS:Ag NRs, back-gate field effect transistors (FETs) based on individual NRs were constructed. The as-synthesized NRs were firstly dispersed onto a SiO_2 (300 nm)–p^+-Si substrate, and then bilayer Cu (4 nm)–Au (60 nm) source and drain electrodes with spacing of ~18 μm were fabricated by photolithography and subsequently a lift-off process. The degenerately doped Si substrate serves as the global back-gate in the nanoFET. To fabricate the p-ZnS NR–n-Si heterojunctions, the SiO_2 (300 nm)–n-Si substrate (0.02 Ω cm) was chosen in this process. An insulative SiO_2 pad (200 μm × 200 μm) on the Si substrate was defined by a photolithography process and subsequently wet etching with a buffered oxide etch (BOE) solution ($HF : NH_4F$ = 1 : 6) for about five minutes at room temperature. After that, the Ag-doped ZnS NRs were dispersed on the substrate, and Cu (4 nm)–Au (60 nm) electrodes that serve as the ohmic contacts to the NRs were defined by additional photolithography process on the insulative SiO_2 pads. The p–n heterojunctions were formed in the contact regions of n-Si substrate and NRs on SiO_2 pads (Fig. 3). All the electrodes materials were deposited by using a high-vacuum electron beam evaporation system.

The device characterization was performed by a semiconductor parameter analyser system (Keithley 4200-SCS) at room temperature. To measure the photoresponse properties of the heterojunction devices, light sources including 632.8 nm He–Ne laser, 254 nm UV light and 850 nm LED, an oscilloscope (Tektronix, TDS2012B), and a mechanical light chopper (LE-oc120) was used.

Results and discussion

Fig. 1(a) shows a typical SEM image of the as-synthesized ZnS:Ag NRs, from which it can be seen that the NRs have width in the range of 200 nm–2 μm, length of 20–100 μm, and thickness of 50–100 nm. The corresponding EDS profile is shown in the inset of Fig. 1(a), the very weak Ag peak suggests that silver element was successfully incorporated into the NRs. From further XRD pattern (Fig. 1(b)), it is seen that the NR can be assigned to be wurtzite structure (JCPDS 80-0007) and no impurity phases are found. Further HRTEM image combined with the fast Fourier transform (FFT) (Fig. 1(c)) reveals that the ZnS:Ag NRs are of single-crystal wurtzite structure, with a growth orientation of $[10\bar{1}0]$. Fig. 1(d) displays a typical CL spectrum of the NRs. It is obvious that the NRs show a strong emission located at ~450 nm, which can be ascribed to the self-activated (SA) luminescence corresponding to the donor–acceptor transition.[22] It has been previously reported that group I metals such as Ag and Cu are fast-diffusing impurities in II–VI compounds, by this token, Ag^+ ions can occupy the Zn^{2+} lattice sites in ZnS and can act as effective luminescent centers which are known to form the so-called blue centers.[23,24] Besides the contribution to optical property, the substitutional doping of Ag^+ in the ZnS NRs by replacing Zn^{2+} could also account for the observed p-type characteristic of the NRs which will be discussed later on.

As we know, ohmic contacts to semiconductor materials or devices are indispensable for solid state device architecture. With the diminishing size of nanostructures based devices, the increasing contact resistance has become one of the most important concerns. According to the Schottky model, the p-ZnS work function, which is about 7.6 eV estimated from the sum of the electron affinity (x = 3.9 eV) and band gap (E_g = 3.7 eV), is so high that there is almost no appropriate metals that can create a barrier-free contact interface without assistance from interfacial reactions or very high near-surface carrier concentrations. The most commonly used method for optimizing the contacts of the wide band gap semiconductors such as p-GaN, p-ZnSe thin films and metals,[25,26] namely minimizing the contact resistance, involves a metallization scheme from bilayer or multilayer metal contact. Enlightened

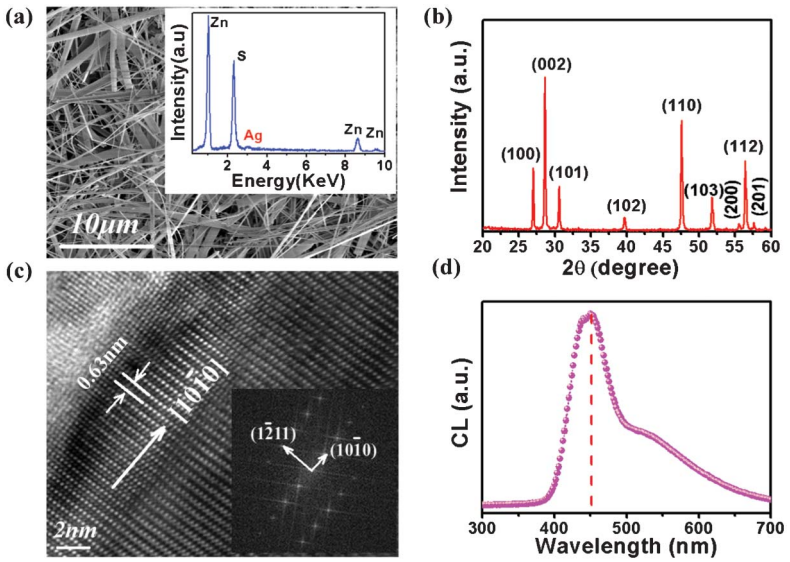

Fig. 1 (a) A typical SEM image of the as-synthesized ZnS:Ag NRs. Inset is the corresponding EDS spectrum. (b) XRD pattern of the ZnS:Ag NR. (c) HRTEM image of the ZnS:Ag NR. The inset shows the corresponding FFT pattern. (d) CL spectrum of the ZnS:Ag NRs.

by this, we develop a new metallization technique which employs a bilayer Cu (4 nm)–Au contact to p-ZnS NR. Fig. 2(a) shows the typical *I*–*V* curves of the p-ZnS NR with Au, Cu, and Cu–Au electrodes, respectively. It is clear that the *I*–*V* curve from the bilayer Cu (4 nm)–Au (60 nm) contact to p-ZnS NRs exhibited linear ohmic behaviour in the as-deposited condition, with a remarkably improved contact to NR. In contrast, either Cu or Au single-layer electrode exhibits much worse contact to the NR even after annealing at 600 °C for 5 min. Specifically, the conductivity of the NRs is remarkably

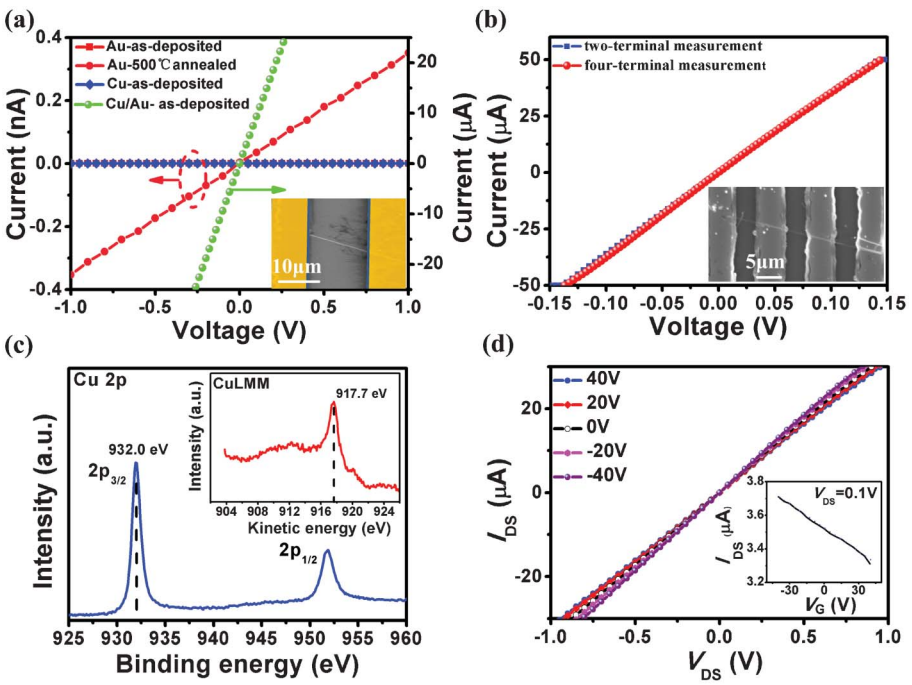

Fig. 2 (a) Typical *I*–*V* curves of the Au, Cu and Cu (4 nm)–Au contacts to p-ZnS NR before and after annealing. Inset shows the SEM image of the device. (b) *I*–*V* curves of a single p-ZnS NR measured by both two-terminal and four-terminal methods with Cu (4 nm)–Au contacts. Inset shows the SEM image of the device for four-terminal measurement. (c) The Cu 2p XPS spectra of the p-ZnS NRs coated with Cu–Au layer. Inset shows the Cu LMM spectra. (d) Electrical transfer characteristics of ZnS:Ag NR based on back-gate field effect transistor, in which Cu–Au electrode were used as the source and drain electrode. I_{DS}–V_{DS} curves plotted at varied V_G from −40 V to 40 V. Inset shows the I_{DS}–V_G curve at V_{DS} = 0.1 V.

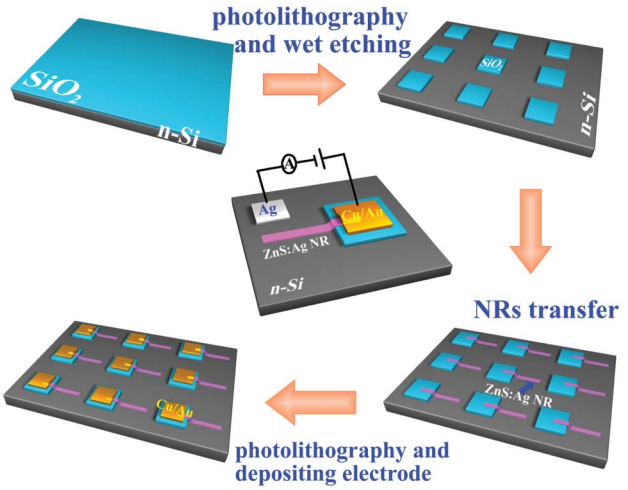

Fig. 3 Schematic illustration of the fabrication process of the p-ZnS NR–n-Si heterojunction PDs.

increased, from 10^{-8} S cm^{-1} for Au or Cu contact to 68 S cm^{-1} for Cu–Au electrode. In order to quantitatively determine the contact resistance between the Cu–Au bilayer electrode and the p-ZnS NR, four-terminal analysis method was employed. Fig. 2(b) shows the *I–V* curves obtained from the two-terminal and four-terminal measurements. It is seen that *I–V* curves measured by these two methods nearly overlapped, revealing the excellent ohmic contact to p-ZnS NR. The contact resistance, as obtained from the difference between the two-terminal and four-terminal resistance values, was estimated to be 20 Ω. Therefore, the specific contact resistivity, one important figure of merit for contact, could be estimated to be $\sim 5.6 \times 10^{-7}$ Ω cm^2 assuming that the whole NR flat is contributing to usable contact area. Comparatively, such a contact resistivity is even lower than the reported value for p-type GaN and ZnSe thin film.[25,27] As we will discuss later, this dramatic decrease in contact resistance could be attributed to the ultrathin Cu film.

In order to unveil the physical origin of the excellent contact of the NR and Cu–Au electrode, we carried out X-ray photoelectron spectroscopy (XPS) and X-ray-induced Auger electron spectroscopy (XAES) analysis. Cu (4 nm)–Au (5 nm) films were firstly coated on the as-synthesized ZnS:Ag NRs in an electron beam evaporator. Then the as-coated NRs were directly transformed into the preparation chamber of the XPS. Fig. 2(c) shows the Cu 2p XPS and Cu LMM spectrum under Ar^+ ion etching for 120 s. The modified Auger parameter (α') is frequently chosen to determine the Cu chemical state. Here, it can be defined as[28]

$$\alpha' = E_k(\text{Auger}) + E_b(\text{photoelectron}) \quad (1)$$

By using Au $4f_{7/2}$ (83.8 eV) as a reference standard, α' is found to be 1849.7 eV from the numerical sum of the Cu $2p_{3/2}$ line (932.0 eV) and the Cu LMM line (917.7 eV). This value is comparable to that of Cu_2S reported previously,[29,30] suggesting the formation of a Cu_2S layer due to surface reaction during electrode deposition. This finding is significant as the unintentional introduction of a thin layer of Cu_2S can greatly reduce the contact resistance by increasing the hole concentration near the surface of NR and decreasing the depletion width of the Schottky junction, which can facilitate the tunneling transport from the p-ZnS NR to Cu–Au electrode by thermionic or thermionic-field emission.

To further characterize the electrical transfer properties of the Ag doped ZnS NRs, the back-gate FETs based on single NR was fabricated. Fig. 2(d) depicts typical gate-dependent source–drain current (I_{DS}) *versus* source–drain voltage (V_{DS}) curves measured at varied gate voltage (V_{GS}) from −40 to 40 V at a step of 20 V. The curve characteristics show the device exhibits an evident p-type gating effect, proving the p-type nature of the ZnS:Ag NRs. The field-effect hole mobility μ_h and carrier concentration n_h are derived to be 154.0 cm^2 V^{-2} s^{-1} and 5.1×10^{18} cm^{-3}, respectively, from the transfer characteristics according to the following equations:

$$g_m = \frac{Z\mu_h C_o V_{DS}}{L} \quad (2)$$

$$n_h = \frac{\sigma}{q\mu_h} \quad (3)$$

where Z/L (500 nm/18 μm) is the width-to-length ratio of the NR channel, C_o the oxide capacitance per unit area, g_m the transconductance of the nanoFET, which can be deduced to $\sim$5.0 nS from inset in Fig. 2(d) according to the relationship of $g_m = dI_{DS}/dV_{GS}$. These results undoubtedly demonstrate that an effective p-type doping has been achieved in the ZnS NRs by using Ag_2S as the dopant. The hole concentration is comparable with the value of the ZnS film.[31] While the high hole mobility of the ZnS:Ag NRs is much higher than that of previous reports for p-type II–VI nanostructures,[32,33] we ascribe this high hole mobility to large channel conduction current in FETs as a result of excellent ohmic contact of Cu–Au electrodes.

The as-synthesized p-ZnS NRs were then used to construct the p–n heterojunction photodiode. Fig. 3 shows the schematic illustration of the fabricating process of the p-ZnS NR–n-Si heterojunction. Briefly, it is mainly composed of three steps. The first step is to define patterned SiO_2 insulator pads by a photolithography and subsequent etching process. The second step is to transfer ZnS NRs to n-Si substrate, and the last step involves fabrication of ohmic contact to NRs on SiO_2 insulator pads. The electrical and optoelectrical properties of the devices was measured between Cu–Au electrode and silver paste.

Fig. 4(a) plots a typical *I–V* curve of the p-ZnS NR–n-Si heterojunction in the dark, exhibiting an obvious rectifying behavior. Careful analysis reveals a turn-on voltage of 0.1 V and a rectification ratio as high as 10^2 in the −1 to +0.5 V range. According to the p–n junction theory, the ideal factor (n) for the device can be determined to be 1.89 from the slop of the forward bias semi-log *I–V* curve shown in Fig. 4(b), according to the following relation

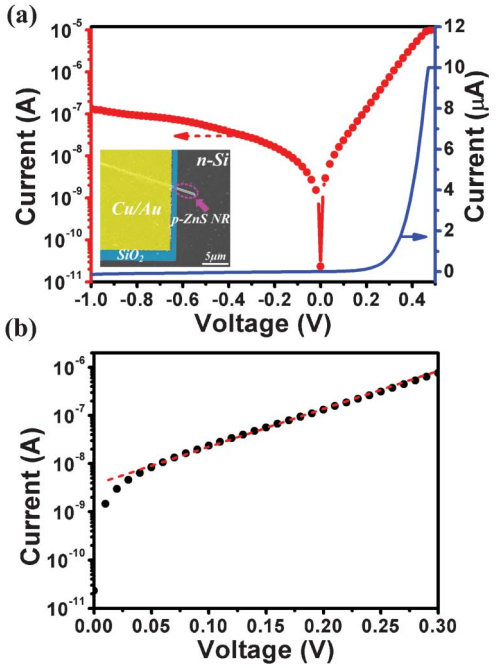

Fig. 4 (a) Typical *I–V* curves of the p-ZnS NR–n-Si heterojunction in both linear and semi-log plot. Inset shows the SEM image of the heterojunction device. (b) *I–V* curve at forward bias.

$$n = \frac{q}{K_B T}\frac{dV}{d\ln I} \tag{4}$$

This value is superior to that of p-SiNWs–ZnO,[16] p-ZnO–n-Si[34] and p-ZnTe NRs–n-Si p–n heterojunctions.[35]

By combining the as-prepared ZnS NRs with n-Si, a photodetector with high sensitivity to ultraviolet-visible-near infrared light can be easily fabricated. To detect the optoelectrical properties of the p-ZnS NR–n-Si heterojunction, the UV light (254 nm), visible light (632.8 nm) and NIR light (850 nm) were chosen and guided onto the device. The light was turned ON and OFF manually to investigate the time response of the PDs. Fig. 5(a) displays the *I–V* curves of the device under the illumination of light with different wavelengths. It can be observed that the p–n heterojunction reveals remarkable photocurrent upon UV-visible-near-IR light irradiation at reverse bias, indicating the high sensitivity of the photodiode to UV-visible-near IR lights. The high sensitivity on reverse bias is consistent with the fact that the photo-excited electron–hole pairs significantly influence the concentration of minority carriers, which dominates the current through a reverse bias.[36] Fig. 5(b) and (c) show the time response of the heterojunction under illumination of light with different wavelengths at reverse bias of −0.5 V. It can be found that the heterojunction PD exhibits high conductance at "light-on" state, but low conductance when the light illumination was switched off, with excellent stability and reproducibility. Further analysis reveals that the photocurrent at light-on and

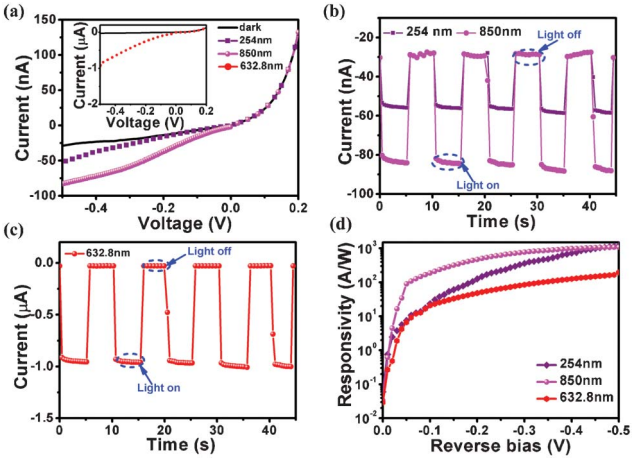

Fig. 5 (a) *I–V* curves of the p-ZnS NR–n-Si heterojunction in the dark and under illumination of UV light (254 nm, 0.4 μW cm^{-2}), visible light (632.8 nm He–Ne laser 100 mW cm^{-2}), inset shows the *I–V* curves of the device under IR light (850 nm 1 mW cm^{-2}). (b) and (c) Time response of the heterojunction under illumination of light with different wavelengths. (d) Responsivity of the heterojunction under illumination of different wavelength of light as displayed in semi-log plot at a reverse bias of 0.5 V.

light-off states are about 1.06 μA and 28.8 nA under 632.8 nm He–Ne laser illumination, respectively. Therefore the current on/off ratio can be estimated to be 36, which is larger than the values of 2 for 254 nm UV light and 3 for 850 nm NIR light. The difference of the current on/off ratio can be attributed to the light intensity. Besides, we also estimated the responsivity (R), a critical parameter for photodetectors. R is defined as the photocurrent per unit of incident power on a photodetector and can be expressed as[9]

$$R(\mathrm{AW}^{-1}) = \frac{I_p}{P_{opt} S} \tag{5}$$

where I_p, P_{opt} and S are photocurrent, incident light intensity and effective illuminated area, respectively. In this study, S is about 5×10^{-8} cm^{-2}. The corresponding R *vs.* reverse bias curves under different light is shown in Fig. 5(d). It is clearly seen that the responsivity for all three different light increases with the increase of reverse bias, and reaches as high as 1.1×10^3, 2.0×10^2 and 1.0×10^3 AW^{-1} for 254, 632.8 and 850 nm, respectively. Interestingly, the responsivity of the device for UV light is larger than that for visible light, which is totally different from what is observed on previous Si-based PDs, where the responsivity for visible light is usually larger than that of the UV light due to the strong absorbing effect. We attribute this high sensitivity to efficient absorption of UV light by the top ZnS NR. The generated electron–hole pairs in depletion region near ZnS NR could be separated under built-in field or applied reverse bias upon UV illumination, giving rise to a large photocurrent in the circuit (Fig. 6(a)). Note that during the light detection process, the applied reverse bias would accelerate the separation of the photogenerated carriers as a result of stronger built-in electrical field. With regard to the higher sensitivity for NIR light than visible light, it is

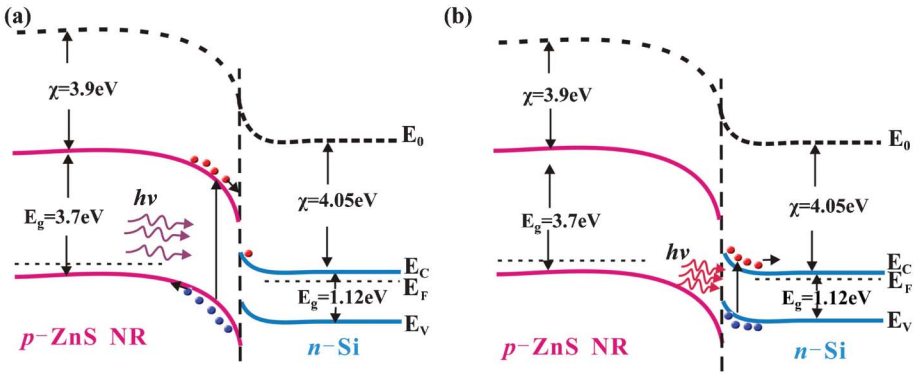

Fig. 6 Energy band diagrams of the p-ZnS NR–n-Si heterojunction upon illumination of UV light (a), and visible and IR light (b) at reverse bias voltage.

probably due to the strong absorption of light in NIR region by the underlying Si. The detailed working mechanism is depicted in Fig. 6(b).

Response speed, which reflects its ability to follow a fast varying optical signal, is another important figure of merit for a photodetector. In our measurements, the photoresponse of the p-ZnS NR–n-Si heterojunction was further probed by an oscilloscope that is capable of monitoring high-frequency switching photocurrent. Note that the pulsed light was generated by a mechanical chopper whose frequency can be automatically adjusted (Fig. 7(a)). Fig. 7(b)–(d) show the time response of the p-ZnS NR–n-Si heterojunction under He–Ne laser illumination with a light intensity of 100 mW cm^{-2}. It is clear that the nanodevice is highly sensitive to the pulsed light in a wide frequency from 50 to 2200 Hz, with excellent stability and reproducibility. Moreover, the $[(I_{max} - I_{min})/I_{max}]$ value only decreases by 40% even at 2200 Hz (Fig. 7(e)), signifying that our device can work at higher frequency. In the time domain, the speed of a photodetector is normally assessed by the rise time (τ_r) and fall time (τ_f) of its response to an impulse signal or to a pulse signal. The τ_r is the time interval for the response to rise from 10 to 90% of its peak value,[5,16,37] while the τ_f is the time interval for the response to decay from 90 to 10% of its peak value. For this device, τ_r and τ_f can be determined to be 48 μs and 180 μs, respectively, under a frequency of 2200 Hz (Fig. 7(f)), which are much faster than those of ZnS NRs and superior to that of reported p–n heterojunction PDs such as p-ZnTe NR–n-Si heterojucntion.[16] Such fast response speed could be attributed to the high quality p–n heterojunction formed between ZnS NR and n-Si substrate, which can facilitate the quick separation of the photo-generated electron–hole pairs. Table 1 summarizes the main device parameters of the p-ZnS NR–n-Si heterojunction and other nano-PDs recently reported for comparison. It notes that our device is much better than not only the devices made of pure ZnS or ZnTe nanostructure, but also the CdTe–Si heterojunction. Understandably, the excellent ohmic contact with negligible contact resistance and the formation of the high-quality heterojunction, due to perfect lattice matching between ZnS and Si, are considered important to good device performance of the p-ZnS NR–n-Si heterojunction PDs. Undoubtedly, this p-ZnS NR–n-Si heterojunction with wide wavelength response, high response speed, high sensitivity will have potential application in future high-performance nano-optoelectronic devices.

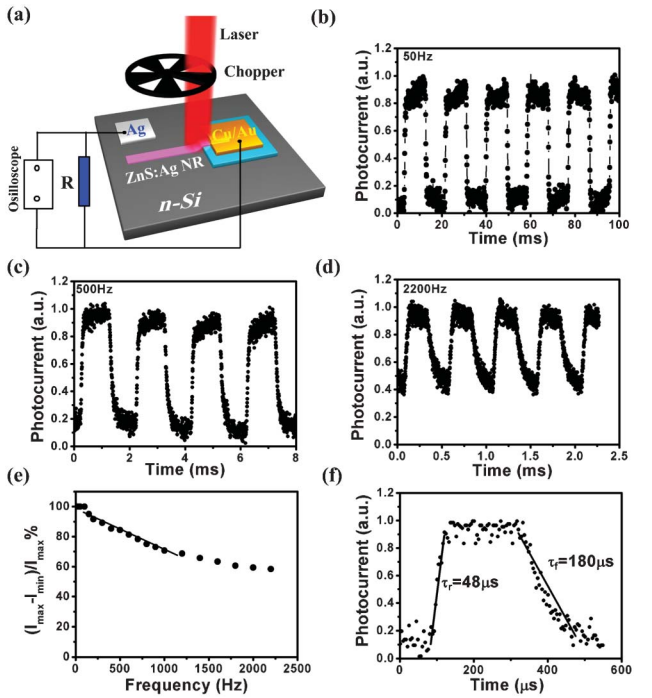

Fig. 7 (a) Schematic illustration of configuration for measuring the time response of the p-ZnS NR–n-Si heterojunction PD. Response characteristics of the heterojunction to the pulsed visible light (632.8 nm, 100 mW cm^{-2} He–Ne laser) at a frequency of (b) 50, (c) 500, (d) 2200 Hz. (e) The relative balance $(I_{max} - I_{min})/I_{max}$ *versus* switching frequency. (f) A single normalized cycle measured at 2200 Hz for estimating both rise time (τ_r) and fall time (τ_f).

Conclusion

In summary, single-crystal p-type ZnS:Ag NRs were synthesized *via* a thermal co-evaporation method. Four-terminal measurement analysis reveals that the Cu–Au bilayer electrode shows

Table 1 Summary of the device performances of the p-ZnS NR–n-Si heterojunction and values of previous reports from other nanoPDs for comparison

Device structure	Rise time (τ_r)	Fall time (τ_f)	Responsivity (AW^{-1})	Ref
p-ZnS NR–n-Si heterojunction	48 μs	180 μs	1.0×10^3	This work
Undoped ZnS NR photoconductor	3 s	3 s	0.2	17
n-ZnS NR photoconductor	95 s	209 s	8.8×10^3	20
p-ZnTe NR–n-Si heterojunction	790 μs	960 μs	1.8×10^3	16
p-CdTe NR–n-SiNWS heterojunction	1.2 ms	1.58 ms		37

excellent ohmic contact to the NRs with specific contact resistivity as low as 5.6×10^{-7} Ω cm^2. The dramatic decrease in contact resistance can be attributed to the formation of the thin Cu_2S interfacial layer between the electrode and NRs, which was verified by both XPS and XAES analysis. Furthermore, the heterojunction PD exhibited high and stable sensitivity to UV-visible-NIR light. The responsivity for 850 nm was as high as 1.1×10^3 AW^{-1} at reverse bias of 0.5 V. What is more, the response speed is as fast as 48 μs, much quicker than other heterojunctions based PDs. These results suggest that such p-ZnS NRs–n-Si heterojunctions will have potential application in future high-performance UV-visible-NIR light photodetection.

Acknowledgements

This work was supported by financial support from the National High Technology Research and Development Program of China (No. 2007AA03Z301), the National Natural Science Foundation of China (No. 20771032, 21101051, 61076040, and 61106010), the National Basic Research Program of China (No. 2007CB9-36001), the Fundamental Research Funds for the Central Universities (2012HGCX0003), and the Foundation of Hefei University of Technology (2011HGXJ1061).

References

1 F. Qian, Y. Li, S. Gradečak, H. G. Park, Y. Dong, Y. Ding, Z. L. Wang and C. M. Lieber, *Nat. Mater.*, 2008, **7**, 701.
2 Y. Huang, X. Duan and C. M. Lieber, *Small*, 2005, **1**, 142.
3 C. Xie, P. Lv, B. Nie, J. S. Jie, X. W. Zhang, Z. Zhang, P. Jiang, Z. Z. Hu, L. B. Luo, Z. F. Zhu, L. Wang and C. Y. Wu, *Appl. Phys. Lett.*, 2011, **99**, 133113.
4 H. M. Wei, H. B. Gong, Y. Z. Wang, X. L. Hu, L. Chen, H. Y. Xu, P. Liu and B. Q. Cao, *CrystEngComm*, 2011, **13**, 6065.
5 J. S. Jie, W. J. Zhang, Y. Jiang, X. M. Meng, Y. Q. Li and S. T. Lee, *Nano Lett.*, 2006, **6**, 1887.
6 L. B. Luo, X. B. Yang, F. X. Liang, J. S. Jie, Q. Li, Z. F. Zhu, C. Y. Wu, Y. Q. Yu and L. Wang, *CrystEngComm*, 2012, **14**, 1942.
7 C. Soci, A. Zhang, X. Y. Bao, H. Kim, Y. Lo and D. Wang, *J. Nanosci. Nanotechnol.*, 2010, **10**, 1430.
8 C. Soci, A. Zhang, B. Xiang, S. A. Dayeh, D. P. R. Aplin, J. Park, X. Y. Bao, Y. H. Lo and D. Wang, *Nano Lett.*, 2007, **7**, 1003.
9 Y. Q. Yu, J. S. Jie, P. Jiang, L. Wang, C. Y. Wu, Q. Peng, X. W. Zhang, Z. Wang, C. Xie, D. Wu and Y. Jiang, *J. Mater. Chem.*, 2011, **21**, 12632.
10 J. Wang, *Science*, 2001, **293**, 1455.
11 O. Hayden, R. Agarwal and C. M. Lieber, *Nat. Mater.*, 2006, **5**, 352.
12 H. Pettersson, J. Trägårdh, A. I. Persson, L. Landin, D. Hessman and L. Samuelson, *Nano Lett.*, 2006, **6**, 229.
13 Y. H. Leung, Z. B. He, L. B. Luo, C. H. A. Tsang, N. B. Wong, W. J. Zhang and S. T. Lee, *Appl. Phys. Lett.*, 2010, **96**, 053102.
14 W. Wang, Q. Zhao, J. Xu and D. P. Yu, *CrystEngComm*, 2012, **14**, 3015.
15 L. B. Luo, F. X. Liang and J. S. Jie, *Nanotechnology*, 2011, **22**, 485701.
16 D. Wu, Y. Jiang, Y. G. Zhang, J. W. Li, Y. Q. Yu, Z. F. Zhu, L. Wang, C. Y. Wu and L. B. Luo, *J. Mater. Chem.*, 2012, **22**, 6206.
17 X. S. Fang, Y. Bando, G. Z. Shen, C. H. Ye, U. K. Gautam, P. M. F. J. Costa, C. Y. Zhi, C. C. Tang and D. Golberg, *Adv. Mater.*, 2007, **19**, 2593.
18 X. F. Wang, Z. Xie, H. T. Huang, Z. Liu, D. Chen and G. Z. Shen, *J. Mater. Chem.*, 2012, **22**, 6845.
19 X. S. Fang, Y. Bando, M. Y. Liao, U. K. Gautam, C. Y. Zhi, B. Dierre, B. D. Liu, T. Y. Zhai, T. Sekiguchi and Y. Koide, *Adv. Mater.*, 2009, **21**, 2034.
20 P. Jiang, J. S. Jie, Y. Q. Yu, Z. Wang, C. Xie, X. W. Zhang, C. Y. Wu, L. Wang, Z. F. Zhu and L. B. Luo, *J. Mater. Chem.*, 2012, **22**, 6856.
21 U. Desnica, *Prog. Cryst. Growth Charact. Mater.*, 1998, **36**, 291.
22 W. P. Jian, J. Q. Zhuang, D. W. Zhang, J. Dai, W. S. Yang and Y. B. Bai, *Mater. Chem. Phys.*, 2006, **99**, 494.
23 T. Suda, K. Matsuzaki and S. Kurita, *J. Appl. Phys.*, 1979, **50**, 3638.
24 T. Suda, K. Matsuzaki and S. Kurita, *Jpn. J. Appl. Phys.*, 1978, **17**, 965.
25 J. S. Jang, I. S. Chang, H. K. Kim, T. Y. Seong, S. Lee and S. J. Park, *Appl. Phys. Lett.*, 1999, **74**, 70.
26 M. Park, W. Anderson, M. Jeon and H. Luo, *Solid-State Electron.*, 1999, **43**, 113.
27 P. M. Mensz, *Appl. Phys. Lett.*, 1994, **64**, 2148.
28 G. Moretti, F. Filippone and M. Satta, *Surf. Interface Anal.*, 2001, **31**, 249.
29 D. L. Perry and J. A. Taylor, *J. Mater. Sci. Lett.*, 1986, **5**, 384.
30 M. Fantauzzi, D. Atzei, B. Elsener, P. Lattanzi and A. Rossi, *Surf. Interface Anal.*, 2006, **38**, 922.
31 E. Bacaksiz, O. Gorur, A. Tomakin, E. Yanmaz and A. Altunbas, *Mater. Lett.*, 2007, **61**, 5239.

32 Q. Peng, J. S. Jie, C. Xie, L. Wang, X. W. Zhang, D. Wu, Y. Q. Yu, C. Y. Wu, Z. Wang and P. Jiang, *Appl. Phys. Lett.*, 2011, **98**, 123117.
33 X. W. Zhang, J. S. Jie, Z. Wang, C. Y. Wu, L. Wang, Q. Peng, Y. Q. Yu, P. Jiang and C. Xie, *J. Mater. Chem.*, 2011, **21**, 6736.
34 J. H. Choi, S. N. Das, K. J. Moon, J. P. Kar and J. M. Myoung, *Solid-State Electron.*, 2010, **54**, 1582.
35 M. Kumar, S. K. Kim and S. Y. Choi, *Appl. Surf. Sci.*, 2009, **256**, 1329.
36 R. Yang, Y. L. Chueh, J. R. Morber, R. Snyder, L. J. Chou and Z. L. Wang, *Nano Lett.*, 2007, **7**, 269.
37 C. Xie, L. B. Luo, L. H. Zeng, L. Zhu, J. J. Chen, B. Nie, J. G. Hu, Q. Li, C. Y. Wu and L. Wang, *CrystEngComm*, 2012, **14**, 7222.

